

















## Supplementary Materials




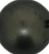












Oyster	Dome	Graft Date	Acq. Start Date	Acq. End Date	Shape
639	1	02/12/2021	02/12/2021	01/03/2022	Atypical
640	2	02/12/2021	02/12/2021	26/01/2022	Other
640	2	02/12/2021	02/12/2021	26/01/2022	Other
643	5	02/12/2021	02/12/2021	26/01/2022	Other
644	6	02/12/2021	02/12/2021	16/12/2021	Other
645	9	02/12/2021	02/12/2021	26/01/2022	Other
646	10	02/12/2021	02/12/2021	26/01/2022	Other
642	4	02/12/2021	02/12/2021	10/08/2022	Round
641	5	02/12/2021	02/12/2021	10/08/2022	Atypical
27	5	02/12/2021	26/01/2022	01/02/2022	Other
28	9	02/12/2021	26/01/2022	19/04/2022	Other
29	10	02/12/2021	26/01/2022	19/04/2022	Other
26	2	02/12/2021	26/01/2022	10/08/2022	Atypical
25	1	02/12/2021	01/02/2022	07/03/2022	Other
644_2	5	02/12/2021	01/03/2022	19/04/2022	Atypical
640_2	1	02/12/2021	07/03/2022	18/05/2022	Atypical
717	10	02/12/2021	19/04/2022	18/05/2022	Other
400	9	02/12/2021	19/04/2022	18/05/2022	Other
25_2	1	02/12/2021	18/05/2022	31/05/2022	Other
27_2	9	02/12/2021	18/05/2022	31/05/2022	Other
188	10	02/12/2021	18/05/2022	10/08/2022	Atypical
903	1	02/12/2021	31/05/2022	09/06/2022	Atypical
904	9	02/12/2021	31/05/2022	10/08/2022	Atypical
905	1	02/12/2021	09/06/2022	14/06/2022	Other
906	1	02/12/2021	14/06/2022	10/08/2022	Atypical
907	1	25/11/2021	10/08/2022	18/08/2022	Round
908	2	25/11/2021	10/08/2022	18/08/2022	Other
909	4	25/11/2021	10/08/2022	18/08/2022	Other
910	10	01/03/2022	10/08/2022	18/08/2022	Atypical
911	5	01/03/2022	10/08/2022	18/08/2022	Other
912	10	01/03/2022	11/08/2022	18/08/2022	Other
913	1	01/03/2022	18/08/2022	11/10/2022	Other
914	2	01/03/2022	18/08/2022	26/09/2022	Other
915	4	01/03/2022	18/08/2022	11/10/2022	Other
916	5	01/03/2022	18/08/2022	11/10/2022	Other
917	9	01/03/2022	18/08/2022	11/10/2022	Round
918	10	01/03/2022	18/08/2022	26/09/2022	Other
919	2	01/03/2022	26/09/2022	03/11/2022	Other
920	10	01/03/2022	26/09/2022	17/10/2022	Other
921	1	01/03/2022	11/10/2022	03/11/2022	Other
922	4	01/03/2022	11/10/2022	03/11/2022	Round
923	5	01/03/2022	11/10/2022	21/10/2022	Other
924	9	01/03/2022	11/10/2022	03/11/2022	Other
925	10	01/03/2022	17/10/2022	03/11/2022	Round
926	1	01/03/2022	03/11/2022	18/11/2022	Round
927	2	01/03/2022	03/11/2022	18/11/2022	Round
928	4	01/03/2022	03/11/2022	18/11/2022	Round
929	9	01/03/2022	03/11/2022	18/11/2022	Round
930	10	01/03/2022	18/11/2022	24/11/2022	Round
931	1	01/03/2022	18/11/2022	24/11/2022	Round
932	2	01/03/2022	18/11/2022	24/11/2022	Atypical
933	4	01/03/2022	18/11/2022	24/11/2022	Atypical
934	9	01/03/2022	18/11/2022	24/11/2022	Other
436	6	02/12/2021	16/12/2021	24/11/2022	Round

Table 1: Table including all the information associated with each oyster: the date of grafting, the start and end dates of acquisition, as well as the final shape attributed. Note that the end date of acquisition also corresponds to the date of sacrifice for the oyster.

 Pearl Number : 25	 Pearl Number : 27	 Pearl Number : 905	 Pearl Number : 26
 Pearl Number : 27-2	 Pearl Number : 400	 Pearl Number : 188	 Pearl Number : 640
 Pearl Number : 639	 Pearl Number : 640-2	 Pearl Number : 641	 Pearl Number : 642
 Pearl Number : 717	 Pearl Number : 903	 Pearl Number : 643	 Pearl Number : 645

(a)

(b)

 Pearl Number : 646	 Pearl Number : 904	 Pearl Number : 912	 Pearl Number : 436
 Pearl Number : 906	 Pearl Number : 907	 Pearl Number : 913	 Pearl Number : 914
 Pearl Number : 908	 Pearl Number : 909	 Pearl Number : 915	 Pearl Number : 916
 Pearl Number : 910	 Pearl Number : 911	 Pearl Number : 917	 Pearl Number : 918

(c)

(d)

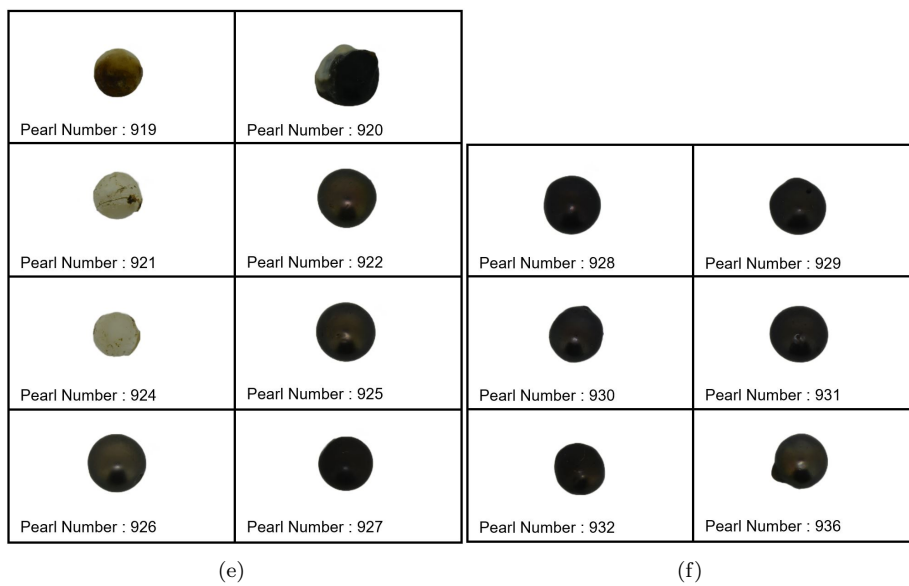


Figure 1: Photographs of all the pearls that were processed by our device are included, except for the 6 pearls that were lost between the characterization and photography stages.

Sensors	C1	C2	C3	C4	C5	C6	C7	C8
X	0.9945	0.7032	0	-0.7320	-0.9945	-0.7032	0	0.7032
Y	0	0.7032	0.9945	0.7032	0	-0.7032	-0.9945	-0.7032
Z	0.1045	0.1045	0.1045	0.1045	0.1045	0.1045	0.1045	0.1045
Sensors	C9	C10	C11	C12	C13	C14	C15	C16
X	0.8660	0.6124	0	-0.6124	-0.8660	-0.6124	0	0.6124
Y	0	0.6124	0.8660	0.6124	0	-0.6124	-0.8660	-0.6124
Z	0.5	0.5	0.5	0.5	0.5	0.5	0.5	0.5
Sensors	C17	C18	C19	C20	C21	C22	C23	C24
X	0.5	0.3536	0	-0.3536	-0.5	-0.3536	0	0.3536
Y	0	0.3536	0.5	0.3536	0	-0.3536	-0.5	-0.3536
Z	0.8660	0.8660	0.8660	0.8660	0.8660	0.8660	0.8660	0.8660
Sensors	C25							
X	0							
Y	0							
Z	1							

Table 2: Cartesian coordinates of each magnetic sensor.

Model	Best Accuracy Obtained
Random Forest	0.515
Naive Bayes	0.468
Simple Logistic Regression	0.422
RBF Network	0.390
OneR	0.203
LSTM	0.441

Table 3: Performance results from various models on our dataset. The best accuracy achieved after optimization is reported, with each accuracy score computed on the test set and represented as the mean of randomized batches. Special care is taken to split oysters into different sets to avoid overfitting. The BioDiscML [22] tool was utilized to calculate all models, with the exception of the LSTM model, which was manually coded and optimized in Python. This table gives an overview of all the results obtained, but it does not include all the models tested.

## Supplementary Note 1: Transformation of our magnet rotation data into real rotation data of the pearl

Let  $M_{magnet}$  be the matrix containing all the magnet orientation data over time, of size  $(T_{tot}, 3)$ . The following are the steps to create the new matrix  $M_{pearl}$ , which corresponds to the orientation data of the pearl, treated as a sphere:

1. For a 3D point  $M_{magnet}(t)$ , which represents the magnet orientation at a certain time, determine two other points at the same time interval:  $M_{magnet}(t - t_{pearl})$  and  $M_{magnet}(t + t_{sphere})$ . In our case, we chose  $t_{sphere} = 1600$  seconds, considering the average rotation speed of our pearls.

2. Calculate the equation of the plane (P1) passing through these three points.
3. Determine the equation of the plane (P2), parallel to the plane (P1) and passing through the origin of the sphere.
4. Determine the plane (P3), perpendicular to both planes (P1) and (P2) and passing through the point  $M(t, :)$ .
5. Calculate the line (D1) that intersects both planes (P2) and (P3).
6. Calculate the two points ( $M_{sphere}^1(t)$ ) and ( $M_{sphere}^2(t)$ ) where line (D1) intersects the sphere representing the pearl. Then, calculate the distances between  $M_{magnet}(t)$  and these two points, and keep the point of intersection that corresponds to the minimal distance, giving the final point  $M_{sphere}(t)$ .

To obtain the new matrix  $M_{sphere}$ , which corresponds to the orientation data of the pearl over time, repeat the six steps outlined above for each point in the matrix  $M_{magnet}$ . The rotation of the pearl over time is finally determined, allowing for the computation of its corresponding velocities and accelerations.

## Supplementary Note 2: Detailed description of our VGG-16 architecture

1. Input layer: This layer receives the RGB image input, which is resized to 224x224 pixels.
2. Convolutional layers: The VGG-16 architecture comprises 13 convolutional layers, each with a 3x3 kernel. These layers extract features from the input image. The number of filters in the convolutional layers increases with depth, starting from 64 and doubling after each max-pooling layer until it reaches 512.
3. Max-pooling layers: VGG-16 includes 5 max-pooling layers, each using a 2x2 kernel with a stride of 2. These layers help to reduce the spatial dimensions of the feature maps, thereby decreasing computational complexity and capturing translation-invariant features. They are interspersed between the convolutional layers.
4. Fully connected layers: After the convolutional and max-pooling layers, VGG-16 has 3 fully connected (dense) layers. The first two dense layers have 4096 units each, followed by three layers with decreasing unit sizes of 1000, 512, and 256, respectively. The size of the final dense layer depends on the number of output classes  $K$  in the classification task, which is 3 in our case. These layers integrate the high-level features extracted by the convolutional layers to make the final classification decision. Each fully connected layer is followed by a 50% dropout layer to prevent overfitting.

5. Activation functions: The VGG-16 architecture employs the Rectified Linear Unit (ReLU) activation function throughout the network, except for the final dense layer, where a SoftMax activation function is utilized to output class probabilities.
6. Output layer: The VGG-16 network’s output layer provides the class probabilities, and the class with the highest probability is chosen as the final classification result.

### **Supplementary Note 3: Detailed description of the entire data handling process, from acquisition to classification.**

1. Input: acquisition of rotation data from the magnet, and oyster information (number of days between graft and acquisition). One sample is equal to one week of rotation acquisition for the pearl.
2. Normalization and filtering of data using a Gaussian-weighted moving average filter.
3. Transformation of magnet rotation data into pearl rotation data, using projections to the equator of a sphere, as described in the Material and Methods section.
4. 3D representation of pearl rotation data, by assimilating the pearl to a sphere.
5. Image acquisition from prior 3D representations, creating 224x224 RGB images of data projected onto a sphere centered on the data’s barycenter.
6. Creation of training, validation, and test sets using the Repeated Holdout method with a 70%/15%/15% split.
7. Output: Training, validation, and test sets are created from filtered, consistent data with added metadata (time elapsed since grafting for acquisition and sacrifice). After filtering outliers due to various acquisition issues, a total of 218 samples from 47 different pearls were retained.
8. Input: Load a pre-trained VGG16 model with custom layers, using weights pre-trained on the ImageNet [20] dataset.
9. Training of the model on our datasets to fine-tune the weights for our images.
10. Hyperparameter optimization using grid search on batch size, learning rate, epochs, and regularization. Evaluation of different models from accuracy and f1-score.

11. Selection of the best model for shape classification on our pearls
12. Input: New rotation data transformed into images as in the training set to be used on our trained model.
13. Output: Final shape prediction of the pearl from new rotation data.

### **Supplementary Note 4: Detailed description of each block from the feature extraction process, from Fig. 6.**

1. Block1-conv1: This is the first layer of the VGG-16 model that detects low-level features such as edges and textures.
2. Block2-conv1: This is the first layer of the second block, where the model starts recognizing more complex patterns like corners and simple shapes.
3. Block3-conv1: The first layer of the third block captures higher-level features, such as object parts and more complex shapes.
4. Block4-Conv1: In the first layer of the fourth block, the model identifies even more abstract features, like parts of objects or specific textures related to the objects in the image.
5. Block5-conv1: The first layer of the fifth block represents the highest level of abstraction in the VGG-16 model. At this point, the model has captured more complex features and patterns that help it differentiate between various objects and scenes. Visualizing this layer offers insights into the model's ability to recognize high-level visual concepts.